

HIGH METALLICITY SOLAR MODEL OR BUST!

Kirsten Howley ¹
Stellar Structure
December 3, 2004

ABSTRACT

We have developed a time independent one solar mass stellar model in hydrostatic equilibrium. The initial conditions imposed on the model are composition and mass; the respective mass fractions used are $X = 0.35$, $Y = 0.55$, and $Z = 0.15$. The star's boundary conditions arise from the equations of stellar structure and yield a radius of 9.791×10^{10} cm, luminosity of 7.521×10^{33} erg/s, effective temperature of 5759 K, central pressure of 1.213×10^{17} Barye, and central temperature of 1.828×10^7 K. Comparison of our model with a grid of high metallicity stellar models developed by Mowlavi results in reasonable correlations between boundary conditions.

1. PARAMETERS OF THE STELLAR MODEL

The construction of a time independent stellar model depends on a variety of both analytic and numerical parameters. These include mass, radius, luminosity, temperature, pressure, composition, opacity, density, nuclear production, and energy transport. The solar model discussed in this paper accounts for all these variables; their interdependent relationships are discussed in detail in the following sections

1.1. Mass & Composition

Mass and composition were the two independent variables in our stellar model. The mass of the star was chosen to be $1 M_{\odot}$, with mass fractions of $X = 0.35$ (hydrogen), $Y = 0.55$ (helium), and $Z = 0.15$ (metals).

1.2. Equations of Stellar Structure: Computing Radius, Luminosity, Pressure, & Temperature

The differential equations for a spherical star can be computed directly from the forces of gravity and pressure acting upon a mass element, and from conservation of energy and momentum. The equations of stellar structure include both a time dependent and time independent component. Since we are considering a star in hydrostatic equilibrium, we can ignore the time dependence and reduce the stellar structure equations to their time independent part,

¹E-mail: kirsten@astro.ucsc.edu

$$\begin{aligned}\frac{\partial r}{\partial m} &= \frac{1}{4\pi r^2 \rho} \\ \frac{\partial P}{\partial m} &= -\frac{Gm}{4\pi r^4} \\ \frac{\partial l}{\partial m} &= \epsilon_n - \epsilon_\nu \\ \frac{\partial T}{\partial m} &= -\frac{GmT}{4\pi r^4 P} \nabla\end{aligned}$$

These four differential equations are coupled and reveal how the four parameters (radius, pressure, luminosity, and temperature) are changing as a function of the enclosed mass. Direct integration of these equations would require knowledge about initial boundary conditions: specifically, the radius and luminosity at the surface and the temperature and pressure at the center. Since the initial boundary conditions are unknown, numerical methods must be employed in order to achieve successful integration. To complicate matters further, ∇ , the energy transport parameter, is also a dependent quantity and must be computed in congruence with the four stellar structure equations.

1.3. Energy Transport

There are three methods for energy transport in a star: diffusion, convection and conduction. Conduction, however, is unable to compete with the efficiencies of radiative diffusion and convection. It has been included in the radiation energy transport equation, but is nonetheless negligible in our model.

In a star, radiative transport can be treated as diffusion, since the mean free path of a photon is much less than the radius of the star. The radiative transport gradient is heavily dependent of the local stellar properties and is given by,

$$\nabla_{rad} = \frac{3}{16\pi acG} \frac{\kappa l P}{m T^4}$$

Convection is also an extremely efficient means of energy transport. It occurs when steep temperature gradients are present, allowing blobs of mass to rise from hotter regions and deposit energy in cooler regions. Convection can also be a source of chemical mixing, oscillations, heating of the chromosphere, and turbulent broadening. However, convection is extremely difficult to model. Mixing length theories are often employed, although they are deemed to be poor approximations. For our model, we have used an adiabatic approximation and the Schwartzchild criterion, without any convective overshoot. The adiabatic approximation yields the gradient,

$$\nabla_{ad} = 0.4$$

and the Schwartzchild criterion states the following condition for convection,

$$\nabla_{rad} > \nabla_{ad}$$

Thus, when ∇_{rad} is less than ∇_{ad} the star is radiative, otherwise it is convective.

1.4. Opacity

In hydrostatic models radiation produced by stars is a result of thermonuclear activity. As the photon leaves its birthplace, it encounters an assortment of particles. Through interactions with these particles, energy can be added to or subtracted from the photon through emissions and absorptions. The mean free path of a photon is defined as the distance it can travel before being absorbed. The opacity, κ_ν , is an absorption coefficient and describes the transparency of the material through which the photon travels. The dependence of κ_ν on frequency makes it very difficult to use numerically (as well as compute), and thus a mean opacity, known as the *Rosseland mean*, is most commonly used. Using κ_ν from atomic physics along with a weighting function, the Rosseland mean computed,

$$\frac{1}{\kappa} = \frac{4\pi}{3\rho} \int_0^\infty \frac{1}{\kappa_\nu} \frac{\partial B}{\partial T} d\nu$$

For our stellar model, we have used a Rosseland mean opacities given by Lawrence Livermore National Laboratory's OPAL opacity tables². The application of these tables to our stellar model will be discussed in further detail in Section 2.

1.5. Density

Pressure support in a star is given by both gas and radiation pressure. Assuming the gas is ideal and the radiation models that of a blackbody, the equation of total pressure can be solved directly for the local density,

$$\rho = \frac{\mu}{\mathfrak{R}T} \left(P - \frac{a}{3} T^4 \right)$$

where a is the radiation density constant, \mathfrak{R} is universal gas constant, and μ is the mean molecular weight. We have assumed for a fully ionized gas which reduces μ to,

$$\mu = \left(2X + \frac{3}{4}Y + \frac{1}{2}Z \right)^{-1}$$

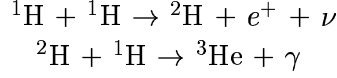
1.6. Nuclear Production: Hydrogen Burning

The luminosity produced in our model is due solely to thermonuclear reactions. High pressures, temperatures and densities allow light nuclei to fuse and form heavier nuclei, releasing energy in the process. The energy produced constitutes a significant portion of the star's pressure support. In our model, we consider two means of hydrogen burning, the proton-proton chain and the CNO cycle.

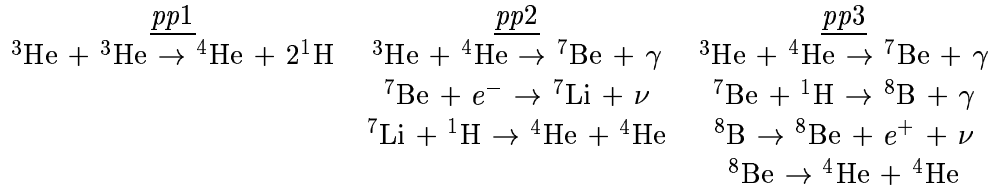
²<http://www-phys.llnl.gov/Research/OPAL/index.html>

1.6.1. Proton-Proton Chain

Hydrogen burning via the proton-proton chain results in the creation of a ${}^4\text{He}$ nuclei from four protons. The energy difference between the initial four protons and final helium nucleus is 26.731 MeV. There are three branches by which the protons can be fused, *pp1*, *pp2*, and *pp3*. The first two steps in each of the three branches are identical,



The first of these two steps is the most crucial in determining the rate of helium production, since it has mean lifetime of 10^{10} years. Once ${}^2\text{H}$ is produced, the reactions proceed in the following manners,



The frequency of each branch is dependent on the local chemical composition, density and temperature of the star. The rate of energy production via hydrogen burning can be calculated from the fusion of the two protons, since the production of the ${}^3\text{He}$ nuclei is the limiting factor,

$$\epsilon_{pp} = 2.38 \times 10^6 \psi f_{11} g_{11} \rho X_1^2 T_6^{-2/3} e^{-33.80/T_6^{1/3}}$$

where ϵ_{pp} and ρ are in cgs units, T_6 is $T/(10^6 K)$, and X_1 is the mass fraction of ${}^1\text{H}$. The factor ψ is an energy correction and can be interpolated from tables. The factors f_{11} and g_{11} are the shielding factor and the correction for non-Gaussian structure of Gamow peak, respectively. The correction g_{11} can be calculated directly, and f_{11} can be reduced to unity if we assume weak screening,

$$g_{11} = \left(1 + 0.0123T_6^{1/3} + 0.0109T_6^{2/3} + 0.0009T_6 \right)$$

$$f_{11} = 1$$

1.6.2. CNO Cycle

Another major hydrogen burning sequence in stars is the CNO cycle. In order for this reaction to occur, carbon, nitrogen, oxygen and hydrogen must be present. The sequence of reactions that occur is given by Figure 1:

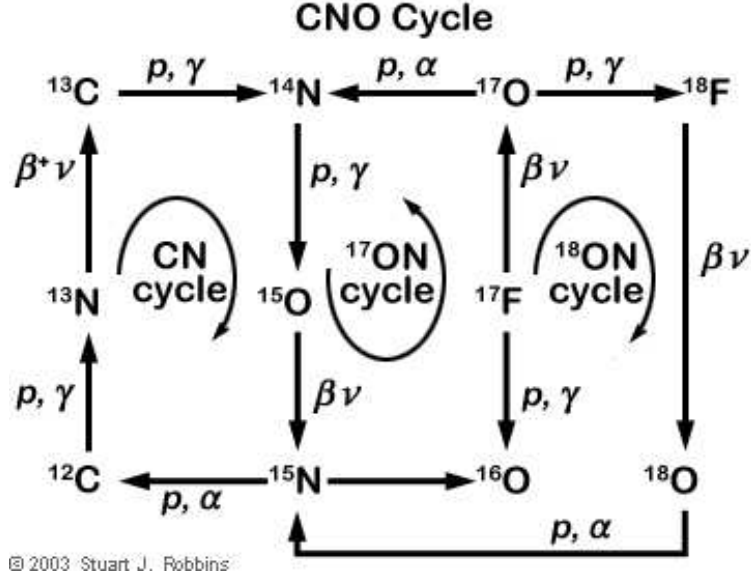
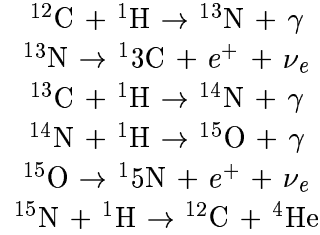


Fig. 1.— Reactions occurring within the CNO cycle.

The most dominant reaction of these reactions (99.96% probability) is,



The limiting factor in this sequence is ${}^{14}\text{N} + {}^1\text{H}$, and thus regulates the rate at which the cycle can be completed. Using this knowledge, the energy generation rate follows,

$$\epsilon_{CNO} = 8.67 \times 10^{27} g_{14,1} X_{CNO} X_1 \rho T_6^{-2/3} e^{-152.28/T_6^{1/3}}$$

where X_{CNO} is the sum of the mass fractions of carbon, nitrogen and oxygen. The correction factor for the non-Gaussian structure of Gamow peak, $g_{14,1}$ is given by,

$$g_{14,1} = \left(1 + 0.0027T_6^{1/3} - 0.00778T_6^{2/3} - 0.000149T_6 \right)$$

The heavy temperature dependence of the CNO cycle means that it will dominate at high temperatures; at lower temperature, the pp chain dominates. These two processes can occur simultaneously in the interior of a star.

2. NUMERICAL COMPUTATION OF THE STELLAR MODEL

2.1. Interpolation: Computing Opacity

The opacity tables given by OPAL provide mean Rosseland opacities at specific temperatures and densities. For this reason, an interpolation had to be made between points in the three dimensional table to determine the opacity. This was accomplished by using IDL's interpolate.pro procedure. Special attention had to be paid to our location on the opacity tables; stringent upper and lower limits were placed on density and temperature.

2.2. Estimating Boundary Conditions

The main goal of this simulation was to find the initial boundary conditions. From surface and central starting values, the intermediate temperature, pressure, radius and luminosity of the star can be derived as a function of mass from the equations of stellar structure.

2.2.1. Inner Boundary

The mass and radius singularities at the center require that a central calculation of temperature and pressure be computed slightly away from the center. A Taylor series expansion of the equations of stellar structure a tiny distance from the origin allow you to compute values close to the center,

$$\begin{aligned}
 r(\Delta m) &= \left(\frac{3m}{4\pi\rho_c} \right)^{1/3} \\
 P(\Delta m) &= P_c - \frac{3G}{8\pi} \left(\frac{4\pi}{3}\rho_c \right)^{4/3} m^{2/3} \\
 l(\Delta m) &= (\epsilon_n - \epsilon_\nu)m \\
 T^4(\Delta m) &= T_c^4 - \frac{1}{2ac} \left(\frac{3}{4\pi} \right)^{2/3} \kappa(\epsilon_n - \epsilon_\nu)\rho_c^{4/3} m^{2/3} \quad (\text{radiative}) \\
 \ln T(\Delta m) &= \ln T_c - \left(\frac{\pi}{6} \right)^{1/3} G \frac{\nabla_{ad,c}\rho_c^{4/3}}{P_c} m^{2/3} \quad (\text{convective})
 \end{aligned}$$

Note that the radiative and convective cases for temperature must be considered separately.

We assigned the value of Δm to be $10^{-5}M_\odot$. The initial central temperature and pressure were set at solar values ($T=1.571 \times 10^7$ K, $P=2.7 \times 10^{17}$ Barye), and later adjusted in the fitting program (Section 2.4). The other variables, radius, luminosity, density, and opacity were self consistently computed with temperature and pressure.

2.2.2. Outer Boundary

The simplest of stellar models assume surface temperatures and pressures of zero. However, the photosphere of stars is much more complex. For this reason, the outer boundary conditions also

had to be self consistently computed. Using initial guesses of solar luminosity and radius ($L=3.9 \times 10^{33}$ erg/s, $R=6.96 \times 10^{10}$ cm), the photosphere temperature and pressure were calculated,

$$T_{\text{photo}} = \left(\frac{L_{\text{photo}}}{4\pi\sigma R_{\text{photo}}^2} \right)^{1/4}$$

$$P_{\text{photo}} = \frac{2}{3}g\kappa_{\text{photo}}$$

where $g = G_c M/R^2$. At the outer boundary, exists an important interdependence between density, opacity and photosphere's pressure. Although we have three relations, and three unknowns, the tabular nature of opacity makes it difficult to analytically solve for these variables. In the numerical simulation, a loop was set up to adjust and recalculate these quantities until they agreed perfectly.

2.3. Integration:

Fifth Order Runge-Kutta Method with Adaptive Step size Control

Numerical integration from the inner and outer boundaries to some point within the star required great precision. It is not only important to have an accurate integrator, but an efficient one also. For this reason, a fifth order Runge-Kutta integrator with adaptive step size was written. The basic equations are laid out below, and the coefficients a_i , b_{ij} , c_i , and c_i^* can be found in section 16.2 of Numerical Recipes:

$$k_1 = \delta m \times f(m_n, E_n)$$

$$k_2 = \delta m \times f(m_n + a_2\delta m, E_n + b_{21}k_1)$$

$$\dots$$

$$k_6 = \delta m \times f(m_n + a_6\delta m, E_n + b_{61}k_1 + b_{62}k_2 + b_{63}k_3 + b_{64}k_4 + b_{65}k_5)$$

Using these k_i coefficients, an estimation of the true solution at a small step size δm away from the initial integration point can be made,

$$E_{n+1} = E_n + c_1k_1 + c_2k_2 + c_3k_3 + c_4k_4 + c_5k_5 + c_6k_6$$

The fourth order Runge-Kutta method is embedded,

$$E_{n+1}^* = E_n + c_1^*k_1 + c_2^*k_2 + c_3^*k_3 + c_4^*k_4 + c_5^*k_5 + c_6^*k_6$$

and an error estimate is given by,

$$\Delta_1 \equiv E_{n+1} - E_{n+1}^*$$

If the desired accuracy, Δ_0 , is known, then a new step size, δm_0 , yielding this accuracy can be derived,

$$\delta m_0 = \delta m \left| \Delta_0 / \Delta_1 \right|^{0.2}$$

Likewise, if the step taken is less accurate than the desired accuracy, adjustments can be made to reduce the step size and the integration from n to $n + 1$ can be recomputed. For our model, an fractional accuracy of 10e-6 was specified.

2.4. Fitting to a Point

The bulk of the work in constructing a solar model is deriving the boundary conditions. Armed with initial guesses and an integrator, convergence at a fitting point within the interior of a star can be tackled. A fitting method, developed by Sears and Brownlee, provides a method by which tiny adjustments can be made to the initial boundary conditions and convergence can be achieved within a desired accuracy.

Integration with initial guesses to a fitting point must first be made. We chose our fitting point to be 2/3 of the mass of the star, and used the following to compute the discrepancies,

$$\Delta Y_j = Y_j^i - Y_j^o \quad (j = 1, 2, 3, 4)$$

where $Y_j^{i,o}$ are the values of the stellar parameters at the fitting point (j indicates the four variables, r , l , P , and T). The superscripts i and o denote the inner and outer boundary conditions, respectively. Small adjustments in the initial boundary values will result in changes in ΔY_j . The discrepancies in each of the variables, Y_j , at the fitting point are given by,

$$\Delta Y_j = \frac{\delta Y_j^o}{\delta E_1} \Delta E_1 - \frac{\delta Y_j^i}{\delta E_2} \Delta E_2 + \frac{\delta Y_j^o}{\delta E_3} \Delta E_3 - \frac{\delta Y_j^i}{\delta E_4} \Delta E_4, \quad (j = 1, 2, 3, 4)$$

Solving this system of four equations for ΔE_j will provide reasonable guesses for the adjustments to the initial boundary conditions. In our model, we used 1/100 of the suggested ΔE_j value, and achieved a convergence to parts better than 1/1000 for each Y_j at the fitting point.

M	R	L	P	T	ρ	κ	ϵ_n	∇
(g)	(cm)	(erg/s)	(Barye)	(K)	(g/cm ³)	(cm ² /g)	(erg/g/s)	
8.84849E+31	6.96942E+09	4.92379E+33	9.31406E+16	1.64455E+07	58.511	2.02998	23.1589	0.4
1.20433E+32	7.7833E+09	5.52733E+33	8.72017E+16	1.60177E+07	56.2474	2.11346	15.344	0.4
1.61937E+32	8.67136E+09	6.03505E+33	8.04578E+16	1.55102E+07	53.6003	2.21441	9.70853	0.4
2.15188E+32	9.64192E+09	6.44092E+33	7.29191E+16	1.49117E+07	50.5332	2.34189	5.96407	0.4
2.49769E+32	1.02052E+10	6.62133E+33	6.85242E+16	1.4549E+07	48.6743	2.42627	4.56655	0.387703
2.84947E+32	1.07398E+10	6.76411E+33	6.43771E+16	1.42088E+07	46.8258	2.5084	3.61001	0.370669
3.66764E+32	1.18777E+10	6.99954E+33	5.5753E+16	1.35034E+07	42.6754	2.687	2.29332	0.338914
4.68004E+32	1.31565E+10	7.18404E+33	4.66351E+16	1.27459E+07	37.8205	2.88973	1.43822	0.30892
5.62382E+32	1.42763E+10	7.29592E+33	3.93458E+16	1.21157E+07	33.5702	3.09829	0.967405	0.289274
6.56765E+32	1.53611E+10	7.37162E+33	3.30092E+16	1.15321E+07	29.5899	3.3117	0.65697	0.273427
8.35969E+32	1.74067E+10	7.45475E+33	2.31179E+16	1.05139E+07	22.7305	3.70382	0.310892	0.246275
9.33713E+32	1.85534E+10	7.47951E+33	1.87161E+16	9.99703E+06	19.3537	3.90633	0.202744	0.2311
1.06477E+33	2.01722E+10	7.4999E+33	1.37483E+16	9.32452E+06	15.2414	4.37198	0.115266	0.22073
1.18942E+33	2.1848E+10	7.51078E+33	9.90085E+15	8.68667E+06	11.7813	4.87771	0.0634258	0.211089
1.3014E+33	2.35249E+10	7.51615E+33	7.09055E+15	8.10824E+06	9.03839	5.40161	0.0346658	0.201707
1.3134E+33	2.37171E+10	7.51655E+33	6.82304E+15	8.04575E+06	8.76483	5.46236	0.0323434	0.200611
1.3134E+33	2.37159E+10	7.51662E+33	6.82315E+15	8.03778E+06	8.77372	5.48141	0.0322162	0.202115
1.3802E+33	2.48407E+10	7.51839E+33	5.44482E+15	7.68316E+06	7.32399	5.91382	0.0214213	0.198388
1.45665E+33	2.62672E+10	7.51968E+33	4.08946E+15	7.2626E+06	5.8188	6.51908	0.0127453	0.194971
1.52466E+33	2.77006E+10	7.52036E+33	3.07027E+15	6.87106E+06	4.61703	7.15886	0.00756268	0.191704
1.58558E+33	2.91611E+10	7.52072E+33	2.29739E+15	6.50269E+06	3.65001	7.83835	0.00445187	0.188277
1.6389E+33	3.06228E+10	7.5209E+33	1.72356E+15	6.16294E+06	2.88886	8.60381	0.00262867	0.18592
1.68596E+33	3.21038E+10	7.521E+33	1.29273E+15	5.84221E+06	2.28533	9.52483	0.00154425	0.185835
1.72771E+33	3.36185E+10	7.52105E+33	9.67038E+14	5.53482E+06	1.80419	10.5637	0.000896891	0.186765
1.76428E+33	3.51527E+10	7.52107E+33	7.23661E+14	5.24156E+06	1.4254	11.7246	0.000516922	0.188862
1.79609E+33	3.66983E+10	7.52109E+33	5.42552E+14	4.96288E+06	1.12846	12.9013	0.000296311	0.190429
1.8239E+33	3.82662E+10	7.52109E+33	4.06689E+14	4.69721E+06	0.893541	14.1011	0.000168384	0.19146
1.8481E+33	3.98528E+10	7.5211E+33	3.04969E+14	4.44419E+06	0.708053	15.4296	9.49072E-05	0.19348
1.86943E+33	4.14821E+10	7.5211E+33	2.27761E+14	4.1981E+06	0.559674	16.9553	5.24576E-05	0.197145
1.8881E+33	4.315E+10	7.5211E+33	1.69478E+14	3.95709E+06	0.44173	18.708	2.83356E-05	0.203018
1.89954E+33	4.43185E+10	7.5211E+33	1.37999E+14	3.79479E+06	0.375012	19.7105	1.82979E-05	0.20469
1.9137E+33	4.59714E+10	7.5211E+33	1.03375E+14	3.57525E+06	0.298112	21.2393	9.78388E-06	0.20815
1.92588E+33	4.76337E+10	7.5211E+33	7.74298E+13	3.36403E+06	0.237267	22.969	5.14622E-06	0.213748
1.93623E+33	4.92855E+10	7.5211E+33	5.81413E+13	3.16036E+06	0.189614	24.9938	2.66356E-06	0.223018
1.94052E+33	5.00549E+10	7.5211E+33	5.08739E+13	3.06748E+06	0.170926	25.4929	1.9444E-06	0.223764
1.94883E+33	5.17242E+10	7.5211E+33	3.80539E+13	2.87371E+06	0.136457	26.6097	9.70669E-07	0.225848
1.95583E+33	5.33774E+10	7.5211E+33	2.85038E+13	2.69104E+06	0.109136	27.7912	4.78533E-07	0.22894
1.96189E+33	5.50576E+10	7.5211E+33	2.12015E+13	2.513E+06	0.0869186	29.1371	2.27349E-07	0.23404
1.96613E+33	5.64304E+10	7.5211E+33	1.6607E+13	2.37337E+06	0.0720831	29.6554	1.21268E-07	0.234016
1.97044E+33	5.80495E+10	7.5211E+33	1.24081E+13	2.21696E+06	0.0576521	30.2436	5.66183E-08	0.233704
1.97403E+33	5.9649E+10	7.5211E+33	9.26434E+12	2.07084E+06	0.0460781	30.7925	2.60631E-08	0.232941
1.97701E+33	6.12222E+10	7.5211E+33	6.91732E+12	1.93493E+06	0.0368173	31.3339	1.18621E-08	0.231848
1.97947E+33	6.27663E+10	7.5211E+33	5.16595E+12	1.8086E+06	0.0294129	31.8921	5.34021E-09	0.230589
1.98154E+33	6.43201E+10	7.5211E+33	3.8283E+12	1.68837E+06	0.023346	32.3907	2.32921E-09	0.228283
1.98285E+33	6.54824E+10	7.5211E+33	3.04661E+12	1.60309E+06	0.0195651	32.6836	1.23109E-09	0.225396
1.98406E+33	6.67222E+10	7.5211E+33	2.37757E+12	1.51628E+06	0.0161405	33.3647	6.13106E-10	0.224218
1.98525E+33	6.81589E+10	7.5211E+33	1.77296E+12	1.41989E+06	0.0128508	34.2972	2.65653E-10	0.223381
1.98623E+33	6.96027E+10	7.5211E+33	1.31053E+12	1.32747E+06	0.0101584	35.2276	1.10907E-10	0.221882
1.98683E+33	7.06344E+10	7.5211E+33	1.05076E+12	1.2642E+06	0.00855112	35.8631	5.8184E-11	0.220115
1.98742E+33	7.18412E+10	7.5211E+33	8.06873E+11	1.19291E+06	0.00695735	36.9468	2.66977E-11	0.219574
1.98797E+33	7.3163E+10	7.5211E+33	5.99529E+11	1.1177E+06	0.00551606	38.2103	1.09749E-11	0.218879
1.9884E+33	7.44507E+10	7.5211E+33	4.45023E+11	1.04729E+06	0.00436867	39.4698	4.44095E-12	0.217669
1.98875E+33	7.57092E+10	7.5211E+33	3.29555E+11	981295	0.00345176	40.652	1.76453E-12	0.215355

M (g)	R (cm)	L (erg/s)	P (Barye)	T (K)	ρ (g/cm ³)	κ (cm ² /g)	ϵ_n (erg/g/s)	∇
1.98902E+33	7.69065E+10	7.5211E+33	2.45391E+11	921477	0.00273621	41.5616	7.09035E-13	0.210813
1.98921E+33	7.79532E+10	7.5211E+33	1.88154E+11	871886	0.00221657	42.6937	3.12039E-13	0.207148
1.98934E+33	7.87758E+10	7.5211E+33	1.51888E+11	834054	0.00186995	44.3112	1.5999E-13	0.20724
1.98945E+33	7.95994E+10	7.5211E+33	1.21948E+11	796972	0.00157072	45.8784	8.00037E-14	0.206634
1.98956E+33	8.05234E+10	7.5211E+33	9.46971E+10	756402	0.00128465	47.9581	3.56898E-14	0.206706
1.98965E+33	8.15338E+10	7.5211E+33	7.11859E+10	713001	0.00102403	50.573	1.41398E-14	0.207537
1.98972E+33	8.24586E+10	7.5211E+33	5.43365E+10	674069	0.000826436	53.1061	5.79328E-15	0.208232
1.98979E+33	8.34715E+10	7.5211E+33	3.99845E+10	632215	0.000648085	56.3364	2.06093E-15	0.210057
1.98984E+33	8.44149E+10	7.5211E+33	2.97058E+10	593831	0.000512357	59.4981	7.39689E-16	0.211737
1.98986E+33	8.50128E+10	7.5211E+33	2.44493E+10	569730	0.000439395	61.8961	3.72655E-16	0.213969
1.98989E+33	8.56671E+10	7.5211E+33	1.96321E+10	543493	0.000369727	64.1979	1.69565E-16	0.215182
1.98992E+33	8.65798E+10	7.5211E+33	1.428E+10	507416	0.000287907	67.5134	5.29381E-17	0.216645
1.98993E+33	8.73174E+10	7.5211E+33	1.09139E+10	478691	0.000233145	69.9121	1.94002E-17	0.216469
1.98995E+33	8.81146E+10	7.5211E+33	8.05657E+09	448302	0.000183678	72.5976	6.14084E-18	0.215711
1.98996E+33	8.88556E+10	7.5211E+33	5.99451E+09	420638	0.000145576	75.438	1.9676E-18	0.215172
1.98997E+33	8.96264E+10	7.5211E+33	4.33988E+09	392431	0.000112899	78.7623	5.5569E-19	0.214693
1.98998E+33	9.02458E+10	7.5211E+33	3.30559E+09	370156	9.11175E-05	81.8405	1.87979E-19	0.214661
1.98998E+33	9.09205E+10	7.5211E+33	2.42194E+09	346221	7.13291E-05	85.9458	5.32429E-20	0.215799
1.98999E+33	9.15869E+10	7.5211E+33	1.75171E+09	322638	5.53248E-05	91.4235	1.37635E-20	0.220155
1.98999E+33	9.22329E+10	7.5211E+33	1.25605E+09	299442	4.27197E-05	98.7449	3.22755E-21	0.229796
1.98999E+33	9.2686E+10	7.5211E+33	9.81797E+08	282527	3.53832E-05	106.104	1.03352E-21	0.243547
1.98999E+33	9.31847E+10	7.5211E+33	7.37385E+08	262797	2.85715E-05	114.725	2.48789E-22	0.264207
1.99E+33	9.36377E+10	7.5211E+33	5.58716E+08	243090	2.34168E-05	125.807	5.35214E-23	0.299847
1.99E+33	9.39455E+10	7.5211E+33	4.56997E+08	227965	2.04421E-05	136.486	1.50976E-23	0.344032
1.99E+33	9.4221E+10	7.5211E+33	3.77355E+08	212265	1.81527E-05	146.01	3.71036E-24	0.4
1.99E+33	9.43071E+10	7.5211E+33	3.54412E+08	207005	1.74911E-05	149.282	2.25852E-24	0.4
1.99E+33	9.46812E+10	7.5211E+33	2.64885E+08	184248	1.47187E-05	157.564	2.13824E-25	0.4
1.99E+33	9.5015E+10	7.5211E+33	1.98167E+08	164056	1.23886E-05	160.791	1.86595E-26	0.4
1.99E+33	9.53128E+10	7.5211E+33	1.48382E+08	146127	1.04298E-05	161.972	1.4956E-27	0.4
1.99E+33	9.55786E+10	7.5211E+33	1.11188E+08	130197	8.78257E-06	171.348	1.097E-28	0.4
1.99E+33	9.5816E+10	7.5211E+33	8.33738E+07	116035	7.39701E-06	194.089	7.3358E-30	0.4
1.99E+33	9.60278E+10	7.5211E+33	6.25547E+07	103439	6.23123E-06	218.545	4.45503E-31	0.4
1.99E+33	9.6217E+10	7.5211E+33	4.69592E+07	92228.7	5.25011E-06	255.783	2.44727E-32	0.4
1.99E+33	9.63859E+10	7.5211E+33	3.52683E+07	82249.2	4.4242E-06	313.83	1.21102E-33	0.4
1.99E+33	9.65368E+10	7.5211E+33	2.6499E+07	73361.8	3.72878E-06	398.866	0	0.4
1.99E+33	9.66715E+10	7.5211E+33	1.99176E+07	65444.4	3.14311E-06	517.757	0	0.4
1.99E+33	9.67919E+10	7.5211E+33	1.49757E+07	58389.2	2.64978E-06	633.961	0	0.4
1.99E+33	9.68993E+10	7.5211E+33	1.12633E+07	52100.7	2.23414E-06	681.299	0	0.4
1.99E+33	9.69953E+10	7.5211E+33	8.47336E+06	46494.3	1.8839E-06	670.181	0	0.4
1.99E+33	9.7081E+10	7.5211E+33	6.376E+06	41495.1	1.58872E-06	654.552	0	0.4
1.99E+33	9.71576E+10	7.5211E+33	4.79878E+06	37036.5	1.33991E-06	671.466	0	0.4
1.99E+33	9.7226E+10	7.5211E+33	3.61238E+06	33059.4	1.13017E-06	696.313	0	0.4
1.99E+33	9.72871E+10	7.5211E+33	2.71975E+06	29511.3	9.53323E-07	704.249	0	0.4
1.99E+33	9.73417E+10	7.5211E+33	2.04798E+06	26345.6	8.04205E-07	688.113	0	0.4
1.99E+33	9.73904E+10	7.5211E+33	1.54235E+06	23520.7	6.78454E-07	660.154	0	0.4
1.99E+33	9.74339E+10	7.5211E+33	1.16169E+06	20999.7	5.72399E-07	651.366	0	0.4
1.99E+33	9.74728E+10	7.5211E+33	875064	18749.6	4.82946E-07	688.192	0	0.4
1.99E+33	9.75075E+10	7.5211E+33	659223	16741.3	4.07491E-07	719.289	0	0.4
1.99E+33	9.75385E+10	7.5211E+33	496661	14948.6	3.43839E-07	651.296	0	0.4
1.99E+33	9.75663E+10	7.5211E+33	374215	13348.3	2.90141E-07	446.434	0	0.4
1.99E+33	9.7591E+10	7.5211E+33	281975	11919.6	2.44837E-07	226.47	0	0.4
1.99E+33	9.76131E+10	7.5211E+33	212484	10644	2.06613E-07	84.2738	0	0.4

4. GRAPHICAL RESULTS

The following graphs reveal the results of our simulation. A brief discussion is given in the caption of each. A more detailed analysis of the validity of our results is given in Section 5.

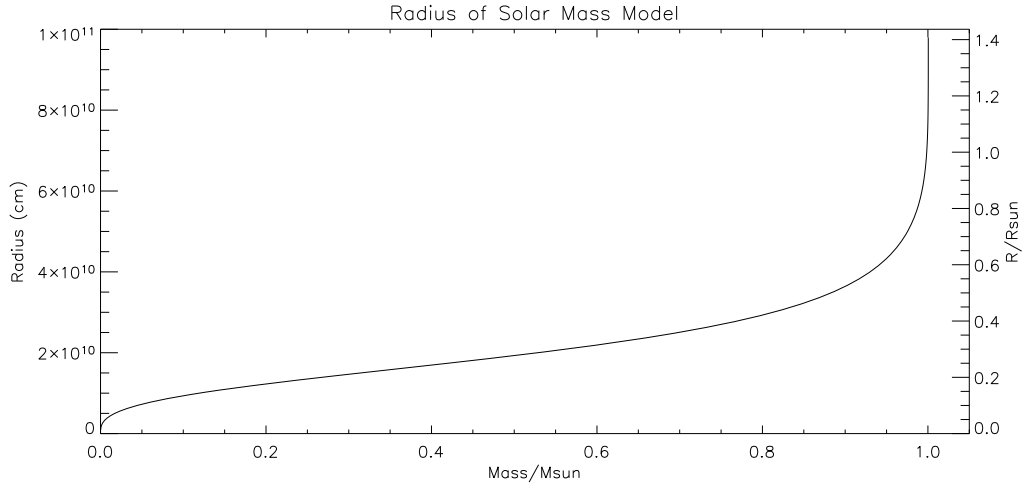


Fig. 2.— Radius of Solar Model. The total radius of our star was found to be 9.791×10^{10} cm ($1.4 R_{\odot}$). The sharp increase in radius in the last couple percent of the mass would be expected for the outer stellar layers.

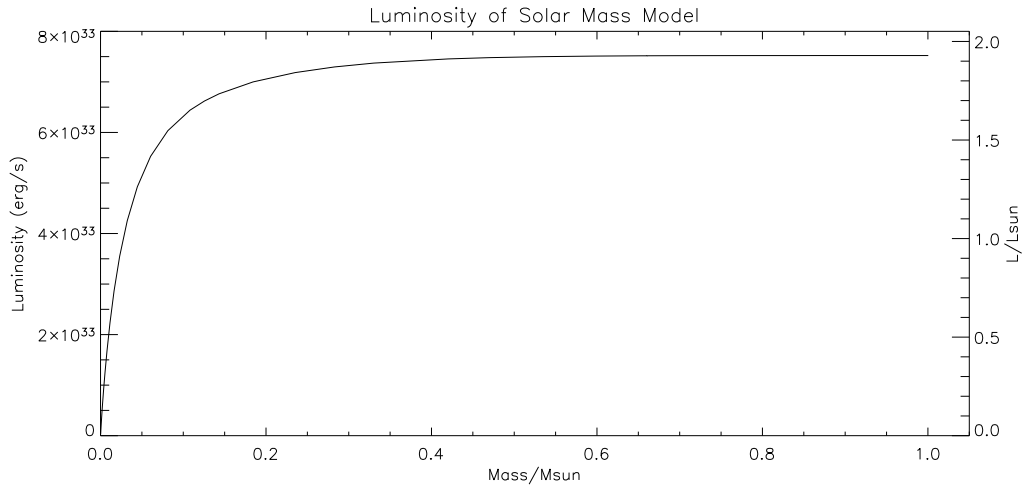


Fig. 3.— Luminosity of Solar Model. The total luminosity of our star was found to be 7.521×10^{33} erg/s ($1.93 L_{\odot}$). The steep gradient near the core correlates with the thermonuclear energy production (see Figure 9).

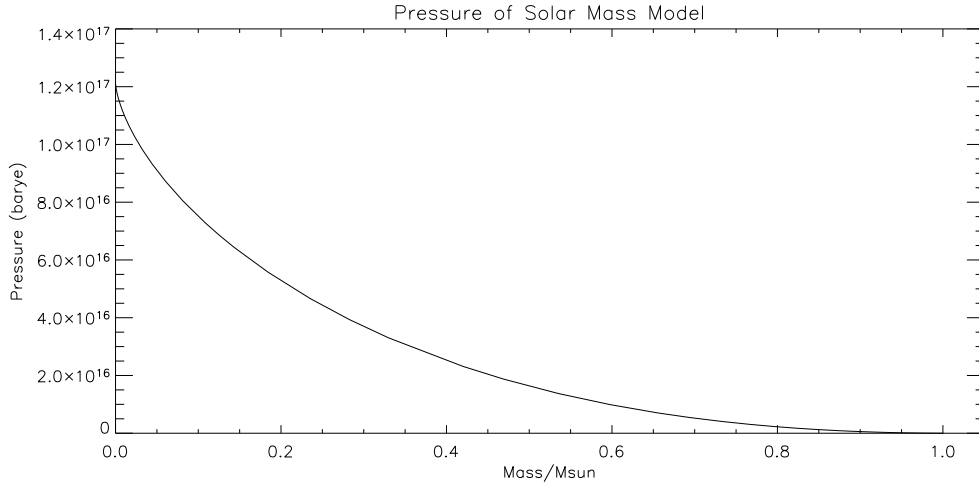


Fig. 4.— Pressure of Solar Model. The central pressure of our star was found to be 1.213×10^{17} Barye ($.45 P_{\odot}$).

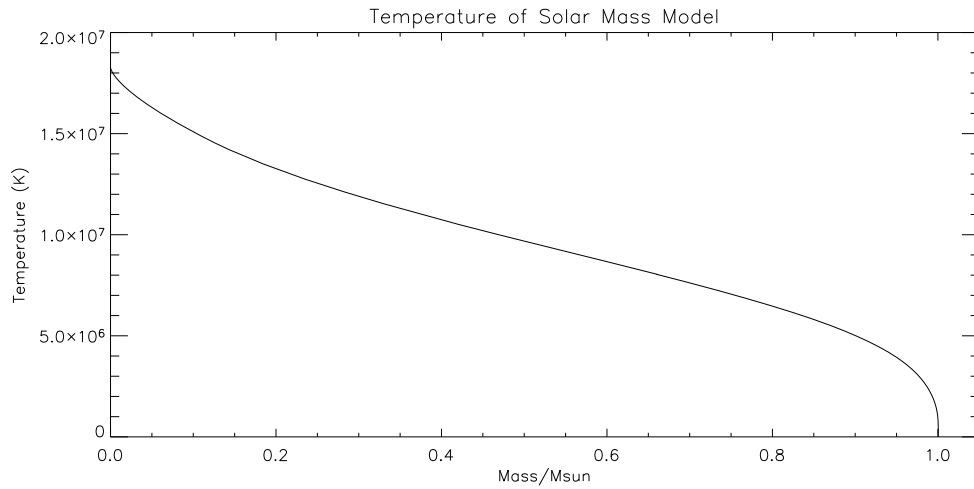


Fig. 5.— Temperature of Solar Model. The central temperature of our star was found to be 1.828×10^7 ($1.16 T_{c\odot}$). Considering the higher metallicity, and thus higher opacity, a core temperature higher than that of the Sun's seems reasonable.

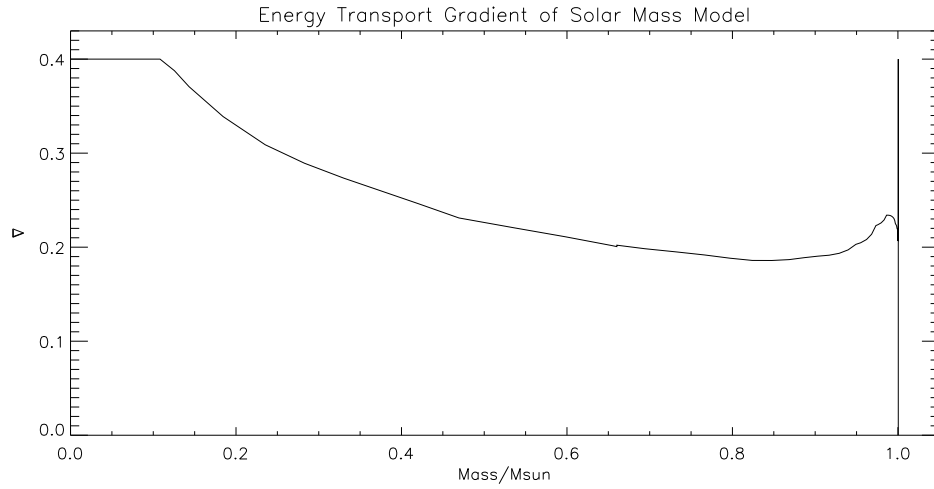


Fig. 6.— Energy Transport Gradient of Solar Model. A core of $0.1 M_{\odot}$ is convective in our model. In addition, there is a small convective envelope just below the photosphere of the star.

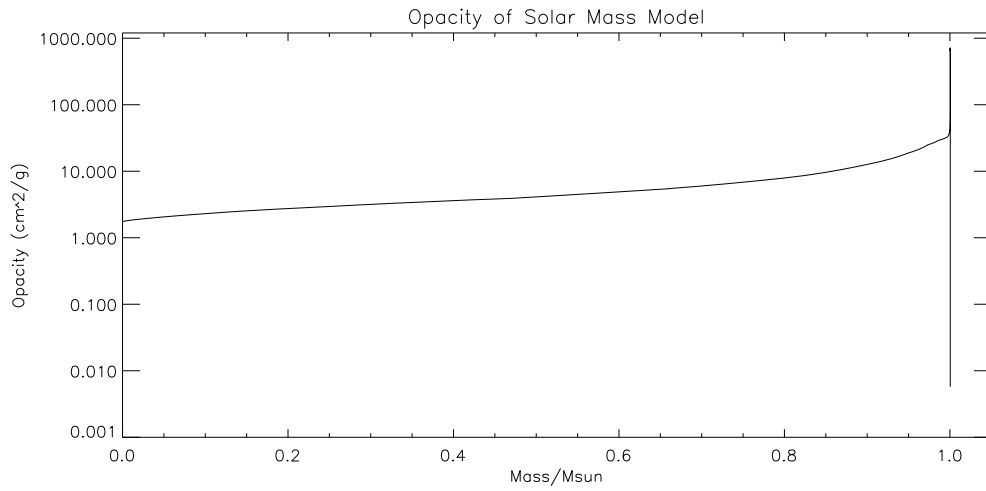


Fig. 7.— Opacity of Solar Model. Opacity changes drastically in photosphere. This is likely a result of various absorption and emission features of the cooler gas.

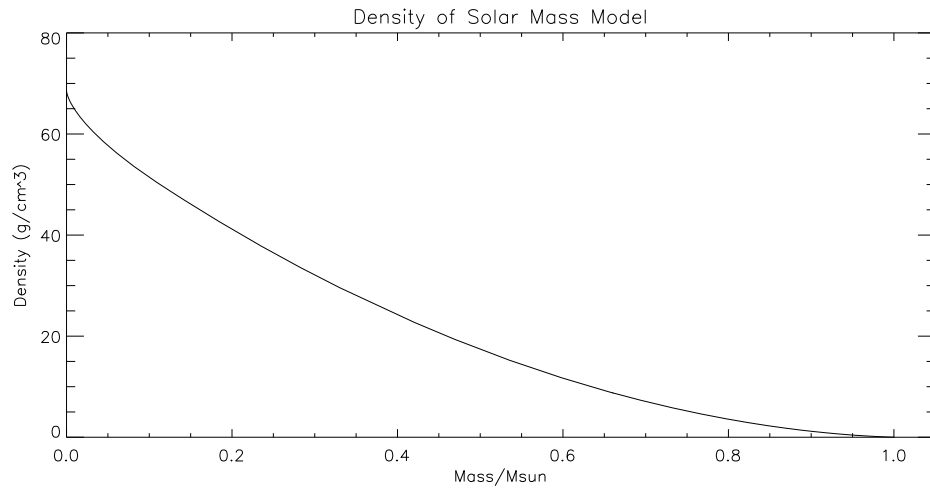


Fig. 8.— Density of Solar Model. Density decreases with increasing mass, as would be predicted.

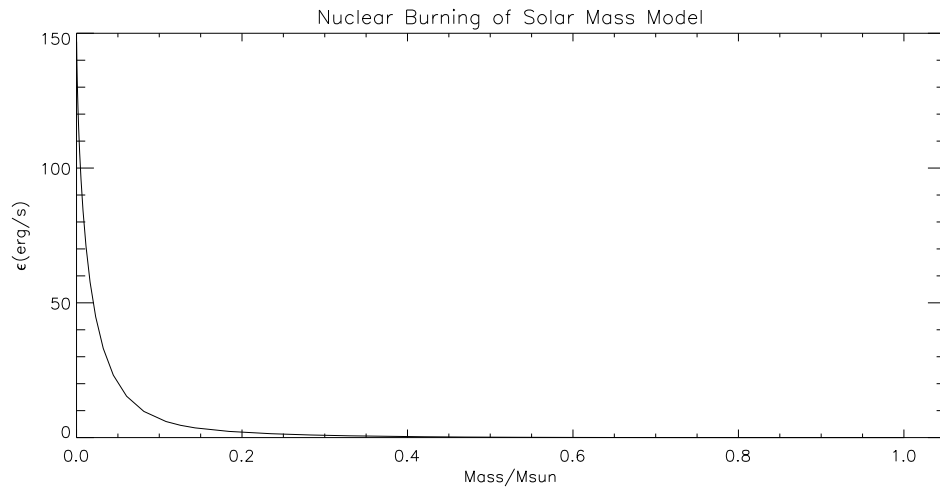


Fig. 9.— Nuclear Energy Generation of Solar Model. Thermonuclear reactions occur mostly within the very hot convective core.

5. MODEL COMPARISON & DISCUSSION

Because astronomers have no physical means of entering a star and making direct measurements, models must be developed and the results compared with observations. However, the particular model that we have chosen has no observational counterpart. Therefore, the high metallicity solar model can only be compared with other models. To accomplish this task, we have chosen to make comparisons with Mowlavi et al (1998). Mowlavi constructed a grid of stellar models with masses ranging from 0.8 to 60 M_{\odot} , and metallicities of $Z=0.10$. Although their Z is 0.05 lower than our $Z=0.15$, it is comparable, and conclusions can be made regarding the plausibility of our model. In addition, Mowlavi has only considered hydrogen burning, which provides an excellent model for comparison with our own.

Below are two figures from Mowlavi's analysis. The important feature to note on the right hand plot is the effective temperature vs. luminosity relationship for a one solar mass star. Our star, with a effective temperature of 5759 K ($0.996 T_{eff\odot}$)k has a luminosity of 7.521×10^{33} ergs ($1.928 L_{\odot}$). Their model, for the same temperature ($\log T_{eff} = 3.76$) results in a luminosity of $1.778 L_{\odot}$ ($\log L/L_{\odot}=0.25$). Furthermore, the graph on the right reveals that if they were to increase their metallicity (i.e. to $Z=0.15$), the luminosity of the star would increase. Thus, our luminosity of $1.928 L_{\odot}$ is very reasonable given our effective temperature.

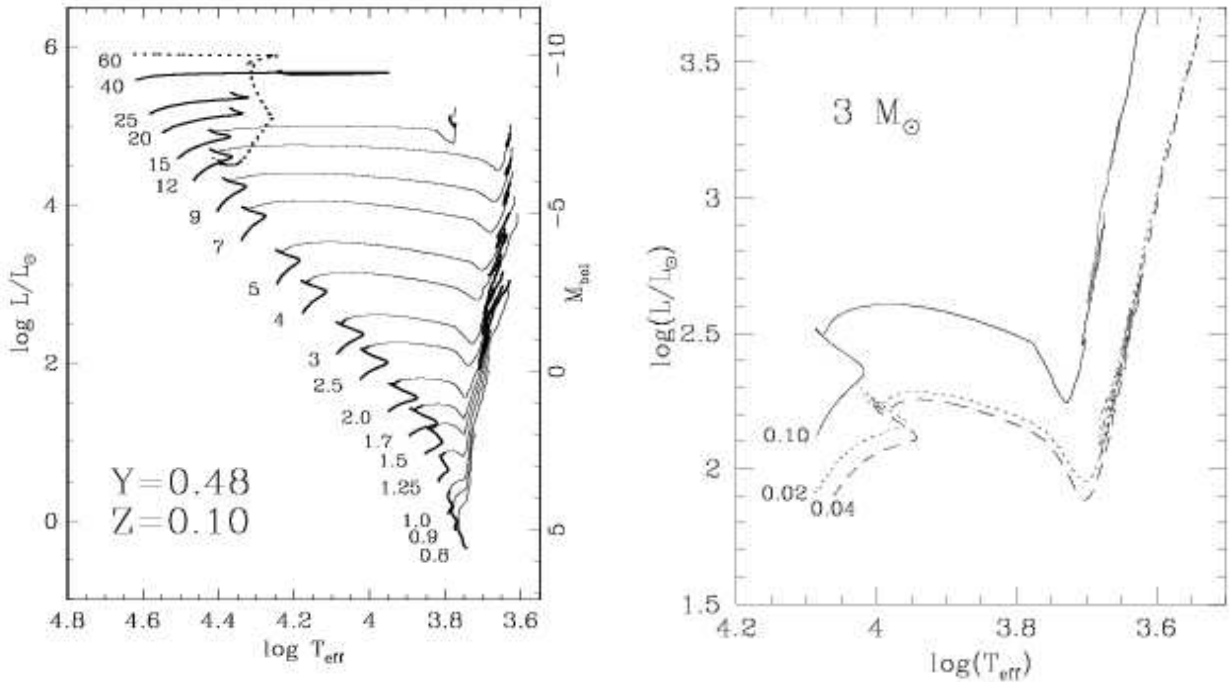


Fig. 10.— Results of high metallicity model from Mowlavi et al 1998 showing T_{eff} as a function of luminosity. The plot on the left shows the increasing luminosity with mass. The plot on the right demonstrates the effect of increasing metallicity.

Figure 11 demonstrates Mowlavi's results for central density as a function of central temperature. Our star, with a central density of 68.375 g/cm^3 has a central temperature of $1.824 \times 10^7 \text{ K}$. Mowlavi's model, for the same density ($\log \rho_c = 1.835$), has an approximate central temperature of 1.66×10^7 ($\log T_c = 7.22$). Our higher central temperature coincides with our higher metallicity; opacity increases with increasing μ and thus more energy is trapped in our core resulting in the higher central temperature.

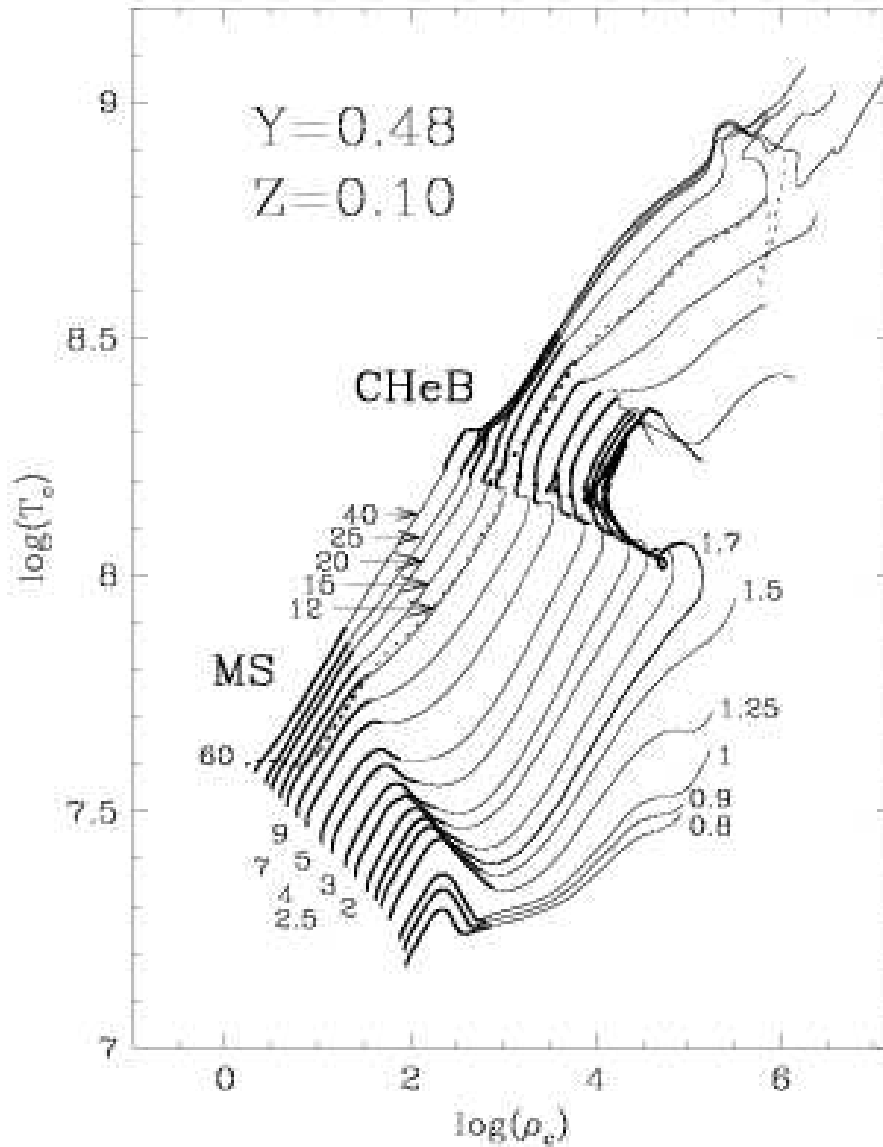


Fig. 11.— Results of high metallicity model from Mowlavi et al 1998. Plot shows central density as a function of central temperature for various stellar models of varying mass.

In Figure 12, Mowlavi has plotted the mass percent of the convective core as a function of metallicity. Low mass stars appear to have a convective cores that are relatively unaffected by metallicity. Although Mowlavi has only one point plotted for a $1M_{\odot}$ star, his $Z/Z_{\odot}=0.7$ results in the same value of $0.1M_{\text{conv}}/M_{*}$ as our $Z/Z_{\odot}=0.87$. This gives us confidence in the size of our convective core.

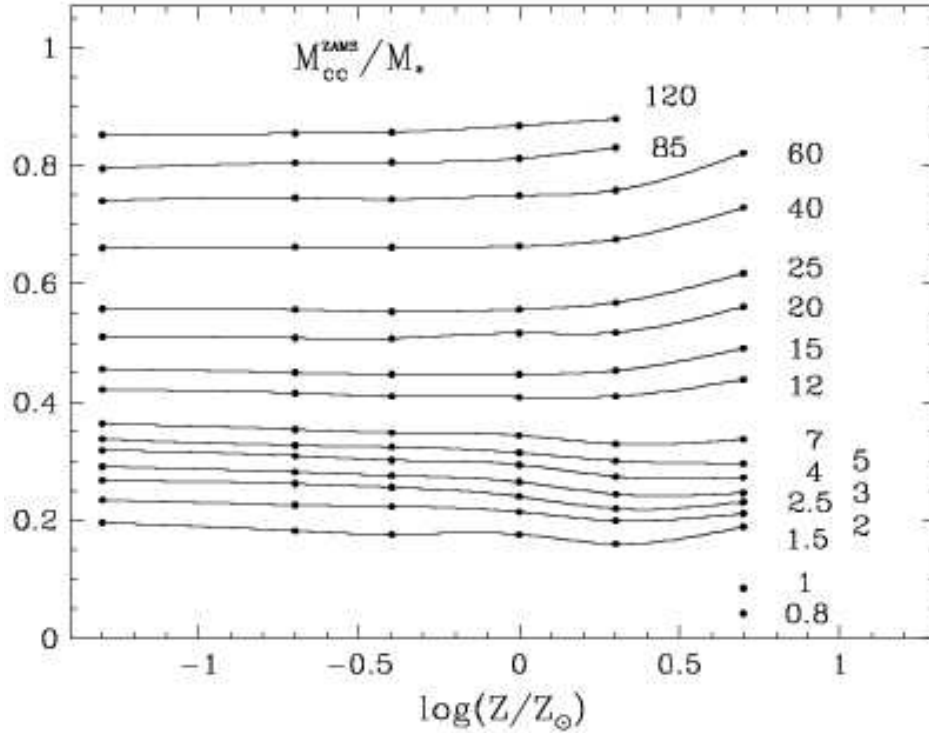


Fig. 12.— Results of high metallicity model from Mowlavi et al 1998. Plot shows convective cores as a function of increasing metallicities for various masses.

Overall, our high-metallicity $1 M_{\odot}$ model compares quite well with Mowlavi's models. This gives us great confidence that we have constructed a reasonably accurate time independent model.

6. COMPUTER CODE

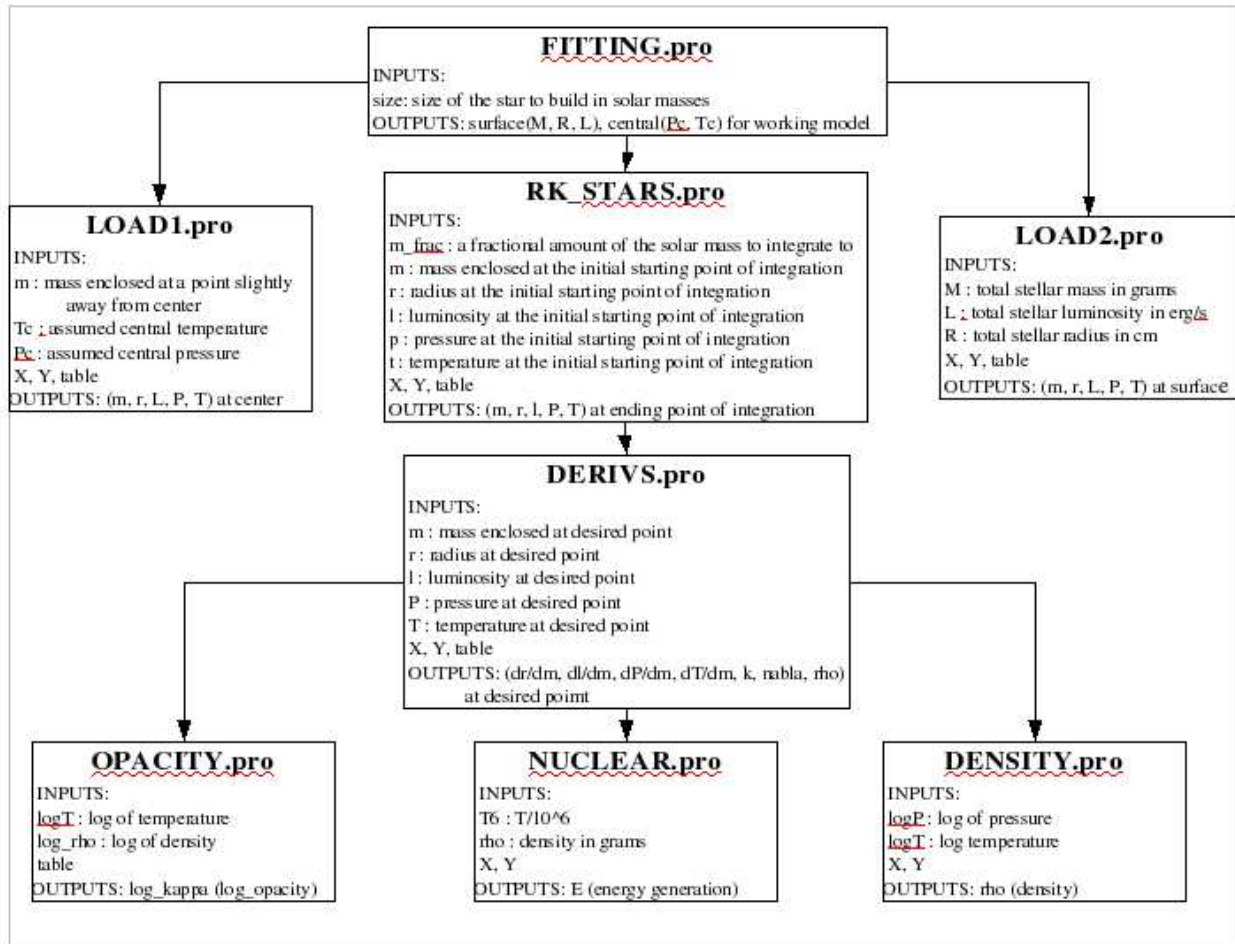


Fig. 13.— Flow chart for programs.

7. REFERENCES

Kippenhahn, R., & Weigert, A. *Stellar Structure and Evolution*. New York: Springer-Verlag, 1994.

Mowlavi, n., Meynet, G., Maeder, A., Schaerer, D., Charbonnel, C., *On Properties of Very Metal Rich Stars*. *Astronomy and Astrophysics* 335, 1998, p. 573-582.

Mowlavi, n., Schaerer, D., Meynet, G., Bernasconi, P.A., Charbonnel, C., Maeder, A., *Grids of Stellar Models VII. From 0.8 to 60 M_{\odot} at $Z=0.10$* . *Astronomy and Astrophysics Supplemental Series* 128, 1998, p. 471-474.

Sears, R., & Brownlee, R. *Stellar Structure - Stars and Stellar Systems: Compendium of Astronomy and Astrophysics, Vol. VIII*. University of Chicago Press, 1965, p. 594-601.